IJICIS, Vol.24, No.4, 82-98
DOI: 10.21608/ijicis.2025.345323.1369

International Journal of Intelligent Computing and Information Sciences

https://ijicis.journals.ekb.eg/

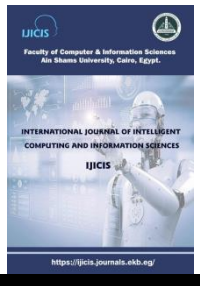

ARTIFICIAL INTELLIGENCE TECHNIQUES IN VISUAL FIELD ASSESSMENT USING HUMPHREY FIELD ANALYSIS: SURVEY

Tasneem I. Abdalgadir*

Computer Science Department,
Faculty of Computer and Information Sciences,
Ain Shams University,
Cairo, Egypt
Tasneem.Idris@cis.asu.edu.eg

Salsabil A. El-Regaily

Basic Science Department,
Faculty of Computer and Information Sciences,
Ain Shams University,
Cairo, Egypt
Salsabil_amin@cis.asu.edu.eg

Thanaa H. Mohamed

Ophthalmology Department,
Faculty of Medicine, Ain Shams University,
Cairo, Egypt
Thanaa@med.asu.edu.eg

El-Sayed M. El-Horbaty

Computer Science Department,
Faculty of Computer and Information Sciences,
Ain Shams University,
Cairo, Egypt
shorbaty@cis.asu.edu.eg

Received 2024-12-17; Revised 2024-12-31; Accepted 2025-01-07

Abstract: *Visual field assessment is a critical component in the diagnosis and management of various ocular and neurological conditions. The Humphrey Field Analyzer (HFA) is a widely used instrument for this purpose, providing accurate and reliable measurements of the visual field. This review explores the principles, methodologies and clinical applications of Humphrey field analysis in visual field assessment and pre-diagnosis of glaucoma using Artificial Intelligence and deep learning. The clinical utility of HFA is demonstrated by its application in the diagnosis and monitoring of diseases such as glaucoma, retinal diseases, and neuro-ophthalmic disorders. In this comprehensive review, the models considered include CascadeNet-5 and Linear Regression, RGC-AC. Each model was trained on a labeled dataset and evaluated using standard performance metrics. Our results demonstrate that CascadeNet-5 outperforms other models in terms of predictive accuracy and sensitivity, while Linear Regression and RGC-AC exhibit comparable performance.*

Keywords: *Artificial Intelligence; Deep Learning; Visual Field; Glaucoma; Humphrey Field Analyzer.*

1. Introduction

It is important to note that glaucoma is the top reason for irreversible blindness [1]. Glaucoma results in the death of Retinal Ganglion Cells (RGCs), leading to a disruption in the transmission of visual information from the optic nerve to the Lateral Geniculate Nucleus (LGN). The Optic Radiations (OR)

***Corresponding Author**: Tasneem I. Abdalgadir

Computer Science Department, Faculty of Computer and Information Science, Ain Shams University, Cairo, Egypt

Email address: Tasneem.Idris@cis.asu.edu.eg

are responsible for transmitting this information from the LGN to the visual cortex. The cells within the LGN are not directly affected by glaucoma, but they experience a lack of sensory stimulation. This deprivation of sensory input may have implications for visual processing in individuals with glaucoma. While glaucoma does not directly impact the cells within the LGN, the absence of sensory input can affect visual processing. This may have consequences for how individuals with glaucoma perceive the world around them. [2]. One of the key questions in sensory neuroscience, with important implications for clinical practice, is whether alterations in the sensory periphery impact the characteristics of central processing pathways [3,4]. Studying the properties of the optic nerve in glaucoma offers a chance to investigate how alterations in the sensory periphery impact central brain connections. Another theory suggests that the effects of glaucoma on white matter may indicate accelerated aging, particularly in the retina [5].

Current approaches to managing glaucoma focus on preventing permanent vision loss and maintaining quality of life. The effectiveness of these strategies is primarily assessed through testing the visual field [6-8]. The Humphrey Field Analyzer (HFA) utilizes the 24-2 test pattern to assess 24 degrees centrally, or the 30-2 test pattern to evaluate a slightly wider area of 30 degrees [9].

At present, the standard clinical method is white-on-white static automated perimetry, which assesses incremental thresholds at different points throughout the visual field [10]. By drawing on both practical experience and historical precedent [11], the 24-2 test grid is commonly used because it includes areas commonly impacted by glaucoma [12], in addition to providing a sufficient number of test locations that are beneficial for clinical use [13]. For instance, a SITA-Faster 24-2 test can evaluate 52 test locations across a visual field spanning about 24 degrees from fixation, including two nasal points, in just 2-3 minutes [14,15].

In recent times, multiple organizations have emphasized the significance of prioritizing visual field testing in the central visual field, specifically within 10 degrees from fixation. This is because defects in central vision can greatly affect daily activities and overall quality of life [16-18].Central visual field defects play a crucial role in modern glaucoma staging systems, as they often indicate the progression of the disease to more severe stages [7,19].Some studies have reported a higher occurrence of central visual field defects when using the 10-2 test [20,21],However, some have proposed that the identification of central visual field abnormalities is comparable across the commonly utilized glaucoma-related visual field test grids, including 24-2, 24-2C, and 10-2 [22-27].

The patient must have undergone visual field testing using the 10-2 (SITA-Fast) and 24-2 (SITA-Faster) protocols on the Humphrey Field Analyzer (HFA3, Carl Zeiss Meditec, Dublin, CA). The results must have met the manufacturer's reliability criteria, as outlined in the authors' previous research, which includes less than 15% false positives or negative, no seeding point errors, and less than 20% of instances with gaze tracker deviations exceeding 6 degrees [28,29].

Artificial Intelligence (AI) is a cutting-edge area of research in computer science that is revolutionizing various medical fields, particularly ophthalmology. AI is expected to significantly impact the diagnosis and treatment of eye conditions like corneal ectasias, glaucoma, age-related macular degeneration, and diabetic retinopathy. However, many medical professionals are unfamiliar with AI concepts and terminology, leading to confusion and misuse of key terms such as machine learning and deep learning [30].

Machine learning and deep learning, two key data-driven pattern analysis methods under the umbrella of AI, have sparked significant interest in recent years. The advancement of technology has led to a surge in AI research for diagnosing ophthalmic and neurodegenerative diseases using retinal images. Different AI techniques, such as traditional machine learning, deep learning, and their combinations, have been utilized for diagnostic purposes [31].

We aim to gain valuable insights into the potential of artificial intelligence to transform the landscape of glaucoma diagnosis by critically evaluating the research and comparing it with the traditional HFA approach. This analysis can flatten the way for improved patient care, earlier intervention, and possibly a future where artificial intelligence is a powerful tool in the fight against vision loss.
The rest of this paper is organized as follows: Section 2 discusses the background check and related works presented in Section 3. Section 4 gives an overview of database resources within the field of ophthalmology. These databases contain valuable information relevant to research and study in this specialized field. These resources serve as important tools for researchers, clinicians, and other professionals working in ophthalmology, offering a wealth of data and knowledge for various applications within the field. Section 5 shows an experimental results discussion and some model experiments. The conclusions and suggestions for future research are showed in Section 6. This section will summarize the findings and propose directions for future studies.

2. Analysis of Humphrey Visual Field 24-2

In this section, we talk about the important points that the diagnosis of glaucoma focuses on based on the results that the device gives us

2.1. Reliability indices

Perimetry results were considered unreliable if they had a false positive rate exceeding 10% - 15%, a false negative rate exceeding 10% - 15%, or more than 20% fixation losses [32,33].

2.2. Total Deviation

The total deviation is determined by comparing the observed threshold to the age-adjusted normal value [34]. The discrepancy between the observed threshold and the normal value adjusted for age is used to calculate the total deviation.

2.3. Pattern Deviation

The numerical values of the pattern deviation numerical plot are calculated by arranging the values from the total numerical plot in chronological order. The seventh highest point in this dataset is then determined. To calculate the numerical values of the pattern deviation numerical plot, the values from the total numerical plot are arranged in a sequential manner. This organization allows for a clear representation of the deviation pattern. By organizing the values in chronological order, researchers can effectively analyze the pattern deviation numerical plot and extract meaningful insights from the data. The methodology employed in this study guarantees a structured framework for comprehending the quantitative data. This approach facilitates a methodical way of analyzing numerical values [35].

2.4. Mean Deviation

The mean deviation measures the extent of vision impairment at each point in comparison to individuals of the same age. It does not take into consideration overall vision impairment caused by other factors like cataracts [36].

2.5. Pattern Standard Deviation

The Pattern Standard Deviation (PSD) gives insight into localized vision loss. A high PSD suggests that the sensitivity loss is not uniform, meaning it is not caused by a general decrease in vision from conditions like cataracts. In cases of advanced glaucoma, the PSD may appear to increase due to decreased overall vision [36]. see Figure. 1 for an example of a Humphrey field examination result.

In this section, we talk about the important points that the diagnosis of glaucoma focuses on based on the results that the device gives us

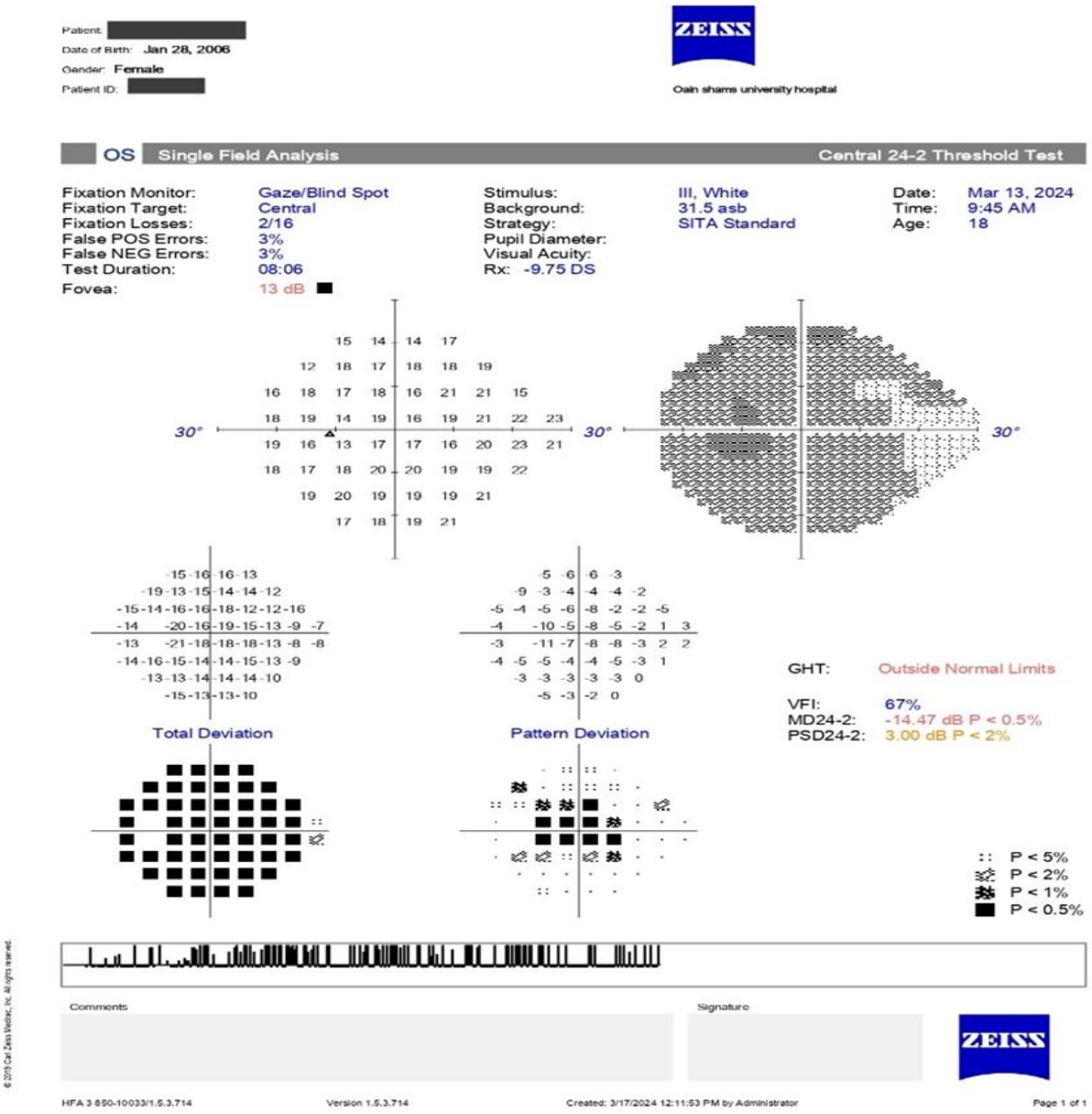

Figure 1: An image showing the examination of a glaucoma patient using the Humphrey device

3. Backgrounds and Related Works

In this section, we will talk about previous literature and classify it according to the type of work

3.1. An Artificial Intelligence Model for Mimicking Visual Phenomena in Order to Assist Individuals Suffering from Visual Field Deficits

In a study conducted by Z. Zhou et al. (2020) [37], deep learning technology and computer vision were utilized to develop an accurate artificial intelligence (AI) model that replicated the effects of visual field (VF) defects observed in patients. Data from Jinan University Affiliated Shenzhen Eye Hospital was collected using the HFA II software, with reliable samples chosen for training. The grayscale map was utilized for the computation of parameters associated with the nature of the damage, as illustrated in Figure 2 A, B. The experimental data included 1,334 normal samples and 1,929 abnormal samples that were considered trustworthy. A sophisticated Convolutional Neural Network (CNN) model was employed to analyze VF damage parameters from input images, achieving an 89% predictive accuracy in identifying VF defect types. By mapping VF damage parameters onto real scene images and adjusting darkening effects accordingly, the visual impact on patients was simulated. Clinical validation revealed no significant differences in the cumulative gray value ($P>0.05$), with 96.0% of average scores rated as good or excellent, confirming the AI model's accuracy.

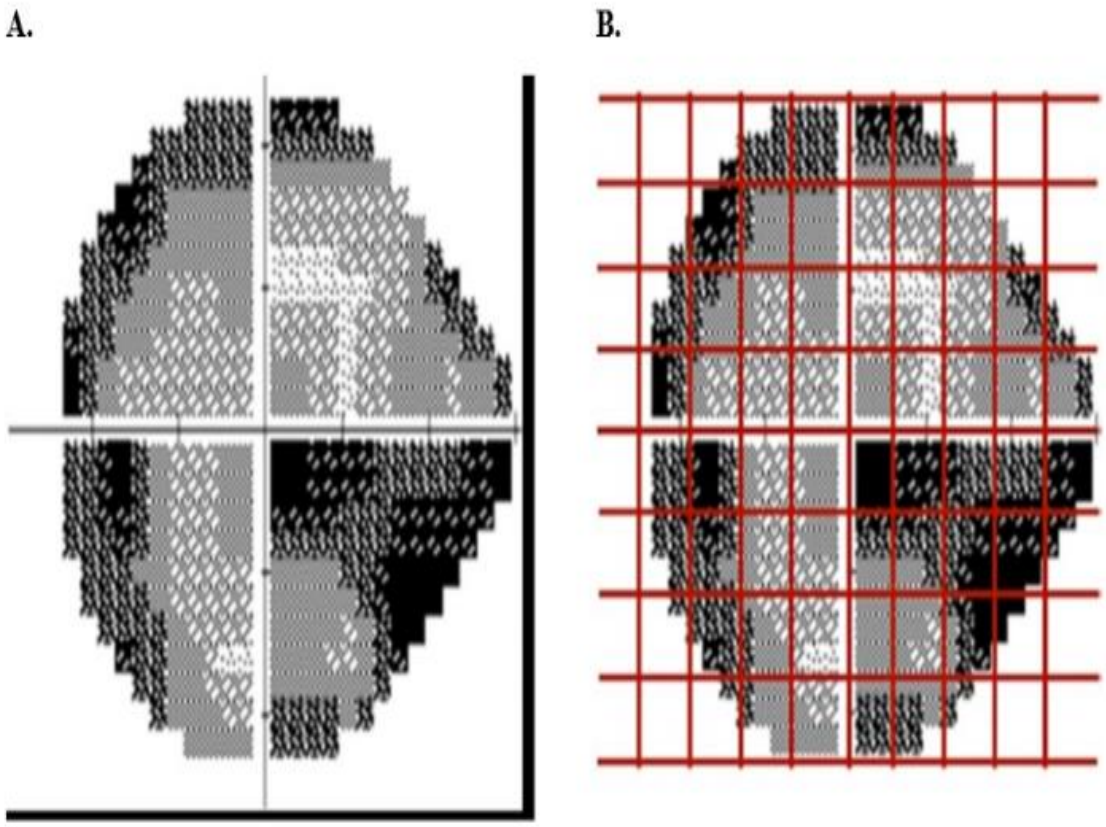

Figure 2 Z. Zhou et al.," shows the grayscale chart of the 24- 2 strategy and the grid processing applied to the grayscale chart. Panel A displays the grayscale chart, while Panel B shows the grayscale chart after grid processing".

3.2. Preclinical Visual Functional Signs of Glaucoma Identification

In their 2020 study, Gupta et al. [38] introduced a framework that utilizes Deep Archetypal Analysis (DAA) to predict the onset of glaucoma several years in advance. This method involves obtaining unsupervised convex representations of visual fields through simplex projections, which are shown to be more clinically meaningful and discriminative compared to traditional visual field analysis methods. To address class imbalance, a class-imbalance bagging approach is implemented. Using the OHTS glaucoma clinical trial dataset as a test case, the study demonstrates that combining deep archetypal representation and class-balanced bagging leads to improved predictions of glaucoma development well before the disease manifests. At the baseline visit, 6,544 visual fields from each eye were deemed reliable and normal according to clinical guidelines. Among these, 724 visual fields were labeled as positive and 5,820 as negative, as illustrated in Figure 3. The mean age of subjects in the negative group was 55.7 years (SD 9.6) and in the positive group was 58.8 years (SD 9.0), with a significant difference ($P < 0.001$) based on Generalized Estimating Equation (GEE) analysis. In the negative group, 42% of subjects were male, while in the positive group, 56% were male, indicating a higher proportion of males developing glaucoma ($P < 0.001$). The mean Intraocular Pressure (IOP) in the negative group was 24.8 mmHg (SD 2.9) and in the positive group was 26.1 mmHg (SD 3.3), with a significant difference ($P < 0.001$). The mean Central Corneal Thickness (CCT) in the negative group was 574.7 mm (SD 38.3) and in the positive group was 558.7 mm (SD 39.0), also showing a significant difference ($P < 0.001$). The study identifies older age, higher IOP, and thinner CCT as risk factors for glaucoma.

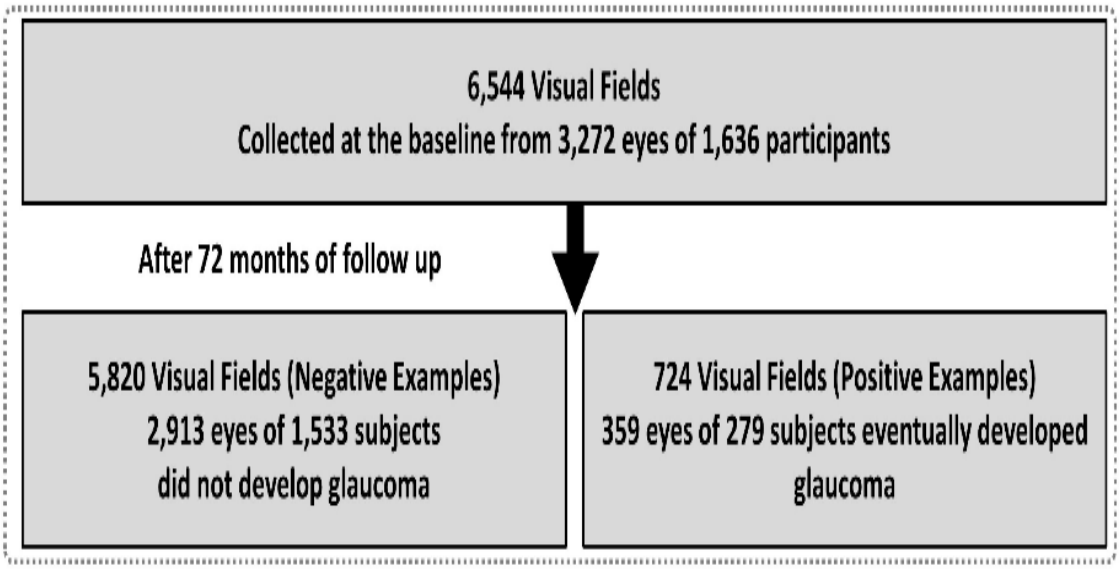

Figure. 3: K. Gupta et al., “Out of 6,544 visual fields analyzed, 5,820 were classified as negative examples, indicating eyes that did not develop glaucoma, while 724 were classified as positive examples, indicating eyes that did develop glaucoma.”

3.3. Predicting the Development of Visual Fields

Predicting the evolution of visual fields is a complex issue involving multiple components and approaches, particularly in the setting of medical illnesses such as diabetic retinopathy, glaucoma, or other ocular diseases.

3.3.1. Humphrey 24-2 Visual Field Thresholds in Glaucoma Patients: Prediction Based on Optical Coherence Tomography Analysis

In a study conducted by Z. Guo et al. [39] (2017), the performance of an enhanced method and three A new class of glaucoma patients was tested via the evaluation of alternative predictive algorithms.The study set up that individual perceptivity thresholds for the Humphrey Visual Field 24- 2 could be prognosticated using Optical Coherence Tomography (OCT) image analysis. Actors passed HVF 24- 2 and 9- field OCT testing, with the whim-whams fiber NFL and Ganglion Cell and Inner Plexiform (GCL IPL) layers segmented into 52 sectors corresponding to the HVF 24- 2 test locations. The study used Wilcoxon rank sum test on assessing the correlation, Root Mean Square Error and Limits of Agreement between predicted and actual thresholds for the four prediction models. The RGC-AC optimized model showed superior results with an R value of 0.74 and RMSE of 5.42 dB, outperforming the Naive, Garway-Heath, and Donut models. Using the RGC-AC idea and 9-field OCT image analysis, the suggested RGC-AC optimized prediction algorithm, demonstrated improved performance and reproducibility compared to previous methods in predicting HVF 24-2 thresholds for glaucoma patients.

3.3.2. Building Deep Learning Predictions about Future Humphrey Visual Fields

In a study conducted by J. C. Wen et al. [40] in 2019, it was found that deep learning networks can effectively learn changes in Spatio-Temporal HVF using unfiltered real-world datasets. These networks were able to predict future HVFs up to five years ahead based on a single HVF input data from 24-2 consecutive HVFs over a twenty-year period were collected from the university database. The researchers used a ten-fold cross-validation approach with a held-out test set to develop the model, focusing on selecting the model architecture, dataset combinations, and training the time-interval model using transfer learning. This led to the creation of an artificial neural network with deep learning capabilities that can produce point-wise visual fields predictions. The accuracy of the predictions was assessed by calculating the Pointwise Mean Absolute Error and the difference in mean deviation between predicted and actual future HVFs. A total of more than 1.5 million perimetry points were analyzed from 32,443 of 24-2 HVFs, with the best model, CascadeNet-5, containing twenty million trainable parameters. The point-wise PMAE for the test set was 2.47 dB, showing a significant improvement over linear model. The 100 fully trained models accurately predicted future HVFs in glaucomatous eyes up to five years ahead, with a correlation of 0.92 between predicted and actual MD values and an average difference of 0.41 dB.

3.4. Other works

3.4.1. Extraction of Automated Reports on Visual Field

In their recent study, M. Saifee et al. (2021) [41] present hvf_extraction_script, an open-source tool developed for rapid and precise automated extraction of data from HVF reports. The tool is designed to simplify the analysis of large HVF datasets and emphasizes the importance of utilizing image processing tools to streamline data extraction in research environments. The validation of hvf_extraction_script involved analyzing 90 HVF reports with different layouts, totaling 1,530 metadata fields, 15,536 value plot data points, and 10,210 percentile data points. A comparison was made between the computer script and four human extractors using DICOM reference data. The study assessed extraction time and accuracy for metadata, value plot data, and percentile plot data. The results revealed that computer extraction took 4.9-8.9 seconds per report, significantly faster than the 6.5-19 minutes required by human extractors.

The error rate for computer metadata extraction ranged from 1.2-3.5%, while human extraction had an error rate of 0.2-9.2% across all layouts. Similarly, computer extraction demonstrated lower error rates for value plot data and percentile data points compared to human extraction. Overall, the study highlights the efficiency and accuracy of hvf_extraction_script in extracting data from HVF reports, underscoring its potential to enhance data analysis in research settings.

3.4.2. PyVisualFields: A Python Package for Visual Field Observation

In their recent study, M. Eslami et al. [42] and colleagues (2023) introduced PyVisualFields, a novel software package aimed at addressing a gap in the field by offering visual field analysis capabilities in Python. This tool has proven to be effective in ophthalmic research for tasks such as statistical analysis, visualization, and predicting visual field progression. With PyVisualFields, researchers can easily develop algorithms for clinical applications using advanced artificial intelligence techniques. Initially, the team compared the functions of R libraries vfprogression and visualFields before translating them into Python using the rpy2 wrapper library. Future versions of PyVisualFields will be independent of R, with upcoming releases already planned. The software is open-source and can be downloaded from the GitHub repository or PyPI. Additionally, various Jupyter notebooks are available to demonstrate the package's features, including data presentation, normalization, plotting, scoring, and progression analysis.

3.4.3. An Open Source, Real-World Set of Perimetry Tests from the Humphrey Field Analyzer

In their 2022 study, G. Montesano et al. [43] created a dataset that allows researchers to access Visual Field (VF) data for various research purposes, such as studying VF behavior, comparing clinical outcomes, and developing new machine learning algorithms. The dataset includes sensitivities extracted from HFA 24-2, stimulus III VFs, and calculations for Total Deviation (TD), mean TD (MTD), pattern deviation, and Pattern Standard Deviation (PSD). Progression analysis was performed using simple linear regression on global, regional, and pointwise values for VF series with more than four tests over at least four months. The dataset comprises 28,943 VFs from 7248 eyes of 3871 patients, with progression data available for 2985 eyes from 1579 patients. The median age of the patients was 64 years, with a follow-up period of more than 2 years. Baseline MTD was -4.51 dB, and baseline PSD was 2.41 dB. Where progression analysis was possible, eyes showed a decrease in MTD of -0.10 dB per year. VFs demonstrating deep localized defects with high PSD values were visually inspected and were found to align with neurologic or glaucomatous VFs. Sensitivity values were compared to printouts for a small number of tests and were confirmed to be accurate.

The next section discusses the evaluation of all the scientific papers mentioned previously and the possible future work that can be done. Table1 presents the outcomes derived by researchers utilizing various models and databases, along with the research objectives they pursued. The researchers employed different models and databases to achieve their research goals.

Table 1 Summary of studies using Humphry visual Field for glaucoma Progression

Author	Year	Aim	Dataset	Model	Results
Z. Guo et al.,[39]	2017	The RGC-AC optimized predictive algorithm, combining 9-field OCT image analysis and the RGC-AC concept,	111glaucoma patients (HVF 24-2 & 9-field OCT)	RGC-AC Garway-Heath Donut Naïve	The study found that RGC-AC, Naïve, Garway-Heath, and Donut had varying degrees of noise reduction.
J. C. Wen et al.,[40]	2019	Deep learning networks them to analyze spatial and temporal variations in HVFs and predict HVFs up to 5.5 years in advance using raw real-world data sets.	Data points were collected from sequential HVF-24-2 between the years 1998 - 2018 in a database at a university.	CascadeNet-5	The test set's point-wise PMAE was 2.47 dB.
K. Gupta et al.,[38]	2020	Create a framework that can predict early signs of vision loss in glaucoma using convex representations derived from the DAA.	A total eye's 6,544 visual fields were evaluated; 724 of these were classified as positive, and 5,820 as negative (30-2 HVFs).	Deep Archetypal Analysis (DAA)	In the negative and positive groups, the mean CCT of the eyes was 574.7 mmHg (38.3) and 558.7 mmHg (39.0).
Z. Zhou et al.,[37]	2020	AI model with high accuracy created to mimic visual manifestations in individuals with visual field defects.	3,263 trustworthy 24-2 HVFs were among the 3,660 HVFs that were gathered as data samples.	VGG19	Up to 89% of the damage type of the VF defects could be predicted with accuracy.
M Saifee et al.,[41]	2021	Introduces hvf_extraction_script, a tool for automated data extraction of HVF reports.	90 HVF reports were validated using three distinct report layouts (10-2, 24-2, or 30-2 test pattern).	Optical Character Recognition (OCR)	A 98% accuracy rate for human extraction and a 99.3% accuracy rate for computer extraction
G. Montesano et al.,[43]	2022	Open access dataset VF dataset	Progression calculation was performed for 1579 patients' 2985 eyes.	linear regression	The baseline PSD was 2.41 dB, and the baseline MTD was −4.51 dB
M. Eslami et al.,[42]	2023	Designed Python package for VF analysis in ophthalmic research.	National Institutes of Health	R libraries Python Language	The developed Python package can be installed from PyPI and is accessible as open-source software.

4. Datasets

Ophthalmology datasets are valuable resources for researchers developing machine learning and artificial intelligence applications in eye care. Here's a breakdown of where you can find them:

4.1. Humphrey Field Analyzer at the University of Washington dataset

The UWHVF dataset is a useful tool for researchers creating new techniques for analyzing VF data and for enhancing the diagnosis and treatment of glaucoma because it includes data from over 28,000 visual field tests [43].

4.2. Harvard Ophthalmology Lab Dataset

Included in the Harvard Ophthalmology AI Lab Datasets, the Harvard FairVision dataset comprises 30,000 samples. Data from 30,000 patients with three main types of eye diseases are included in this [44].

4.3. A Brazilian Multilabel Ophthalmological Dataset

This dataset provides a collection of retinal images from a Brazilian patient population and is accessible on PhysioNet. More than 16,000 photos from more than 8,500 patients are included in it [45]. Details for each of the datasets mentioned are displayed in Table 2.

Table 2: Comparison between the publicly available ophthalmology datasets.

Dataset Name	No. of Sample	Contain
UWHVF dataset	28,943	Advancement Pointwise sensitivities, excluding patient age, gender, and laterality were extracted from HFA 24-2 visual fields.
Harvard Ophthalmology AI Lab Dataset	30,000	This includes the three primary eye conditions of glaucoma, diabetic retinopathy and age-related macular degeneration.
A Brazilian Multilabel Ophthalmological Dataset	16,266 images	Color fundus retinal photos are included, along with quality control artifacts, focus, illumination, image field, and anatomical parameters of the macula, optic disc, and vessels.

5. Experimental Result and Discussion

5.1. Experimental Results

This section presents the results of our comparative study on the performance of three models: RGC-AC, CascadeNet-5, and Linear Regression. The primary objective was to evaluate these models on key performance metrics in the context of visual field screening in glaucoma patients using Humphrey field analysis. It is applied to each study separately and the results are presented.

This section presents the results of our comparative study with previous studies using the UWHVF dataset. The primary objective was to evaluate the effectiveness of the model in terms of accuracy. The dataset used in this study is the UWHVF, which contains 2985 eyes from 1579 patients.

The RCC-AC model is evaluated using 3-fold fitting to each of the 108 candidates, for a total of 324 RGC-AC fits $R = 0.91$.

We used the Matplotlib library and the Seaborn library to draw charts that help in analyzing the performance of the prediction model, as the dots scattered in blue represent the true values on which the model was tested versus those that the model predicted based on the input data. Through this chart, we can see how close the predicted values are to the true values, as shown in Figure 4.

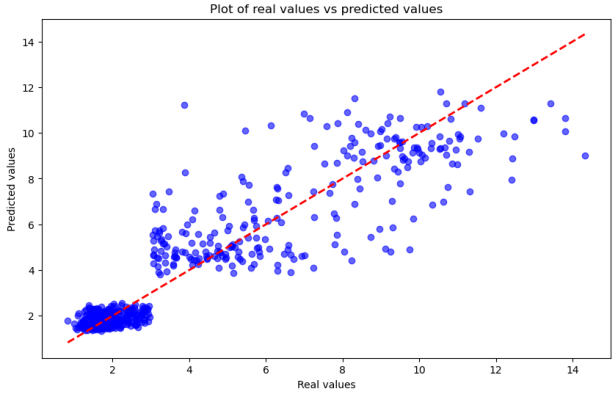

Figure 4: Real Value vs Predicted Value

Errors, which are the differences between the true values and the expected values, were calculated with the probability density curve in purple bars shown in Figure 5. Our understanding of this model's performance indicates that the model predicts the values accurately on average because the distribution is centered around zero. In the pattern analysis, there were no long tails in either direction. This indicates the absence of some predictions that are very far from the true values. This chart provides a visual way to understand the distribution of errors made by the model, and is an essential part of evaluating model performance in machine learning.

Residuals are visually distributed in orange in Figure 6, making it easier to understand how spread out the values are. The chart displays outliers as individual marks that lie outside the "whiskers" extending from the box.

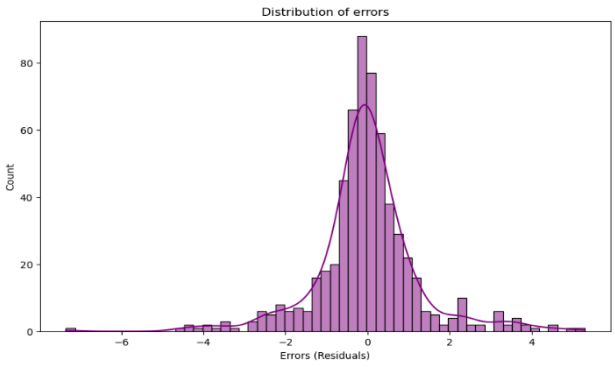

Figure 5: Distribution of Errors

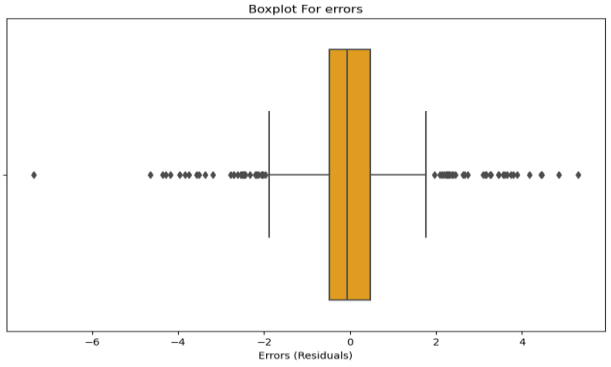

Figure 6: Boxplot for errors

The CascadeNet-5 model is evaluated and the performance accuracy was 98% compared to the accuracy mentioned in the study 95% [40]. Figure 7 illustrates the confusion matrix where the upper-left box represents points that were correctly classified as "positive" and actually have a positive value, the upper-right box represents points that were incorrectly classified as "negative" and actually have a positive value, and the lower-left box represents points that were incorrectly classified as "Negative" and actually have a negative value, the lower right box lists points that are correctly classified as "Negative" and actually have a negative value.

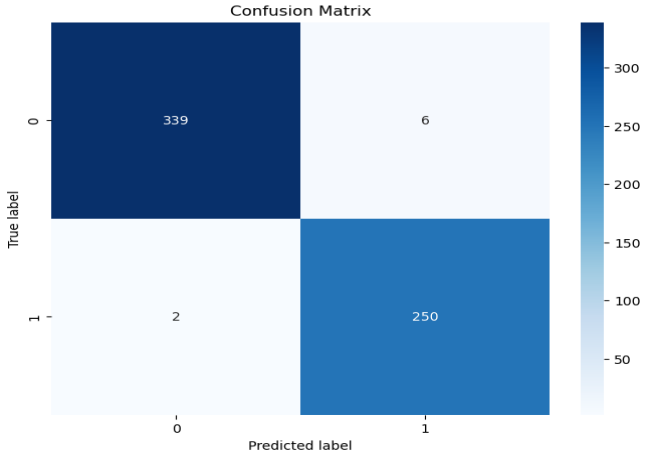

Figure 7: An image showing the positive value and negative value

The linear regression model was evaluated and the results were obtained RMSE (Root Mean Squared Error): 0.29, R^2: 0.64.
The matplotlib.pyplot library was used to create the graph. The scatter lines shown in blue show actual values versus predicted values. A line was drawn representing the ideal relationship where the expected values should be equal to the actual values. Points were placed on the horizontal and vertical axes to define the range of the line. This ensures that the line extends from the minimum to maximum of the actual values and sets the line color to red. Figure 8 shows a plot of actual and expected values.

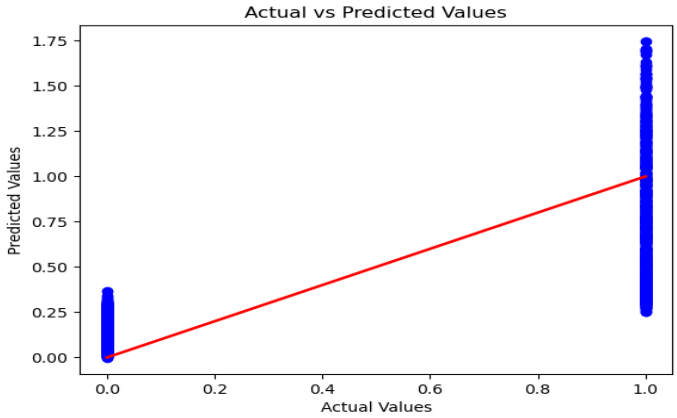

Figure 8: The plot of actual and forecast values.

The analysis involved comparing findings from prior studies utilizing the UWHVF databases. The table displays the specific model that underwent testing. Overall, our investigation included a comparison of outcomes from earlier research conducted with the UWHVF databases [43]. The table 3 presents the model that was subjected to testing.
Each of the studies mentioned has a different purpose; however, the outcomes all pertain to results derived from the HVF device. They may, therefore, differ in what they precisely seek to ascertain, yet they are similar in the aspect of measuring effects of the HVF device.

Table 3: Comparison of previous studies using Humphrey visual field for glaucoma progression

First Author	Dataset	Model	Result	The Model Used	Dataset Used	Evaluation
Z. Guo et al., [39]	XNAT ophthalmology research database	RGC-AC	RGC-AC (R = 0.74,95% CI, 0.67–0.76)	RGC-AC	UWHVF dataset	RGC-AC (R = 1.25 dB; 95% CI, 1.12–1.37 dB)
J. C. Wen *et al.*, [40]	Data collected from sequential HVF-24-2 between the 20 years in a database at a university.	CascadeNet-5	Accuracy: 95%	CascadeNet-5	UWHVF dataset	Accuracy:98%
G. Montesano *et al.*, [43]	UWHVF dataset	Linear Regression	The baseline PSD was 2.41, and the baseline MTD was −4.51.	Linear Regression	UWHVF dataset	RMSE: 0.2961621880350672 R^2: 0.6404260289584186

*5.2.*Discussion

Recent advancements in artificial intelligence (AI) have shown promising applications in the field of ophthalmology, particularly in the analysis of Humphrey visual field tests and the diagnosis of glaucoma. A comprehensive survey conducted on the utilization of AI in these areas revealed that machine learning algorithms, especially deep learning models, significantly enhance the accuracy and efficiency of detecting visual field defects and glaucomatous progression. The integration of AI in Humphrey field analysis not only reduces the subjectivity associated with traditional methods but also provides a robust framework for early diagnosis and monitoring of glaucoma, potentially improving patient outcomes through timely intervention.

In this study, we employed three distinct models to analyze the UWHVF dataset: Linear Regression, RGC-AC, CascadeNet-5, and Linear Regression. Each model was selected for its unique strengths and potential to offer diverse perspectives on the data.The RGC-AC analysis results ranged from 1.12–1.37 dB with a 95% confidence interval, with a mean observed change of 1.25 dB. This suggests that the expected change in the relationship between the retinal ganglion cells (RGC) and the anterior chamber (AC) is within these limits, providing important insights into how glaucomatous changes affect RGCs. These results highlight the importance of understanding the effects on retinal ganglion cells in the development of glaucoma.

As for the performance of CascadeNet-5, it showed an exceptional accuracy of 98%. This result is pivotal in sensitive fields such as glaucoma diagnosis, where accurate data classification is of paramount importance. These results confirm the model's ability to correctly classify data, highlighting its effectiveness in clinical applications.

On the other hand, the linear regression analysis results showed an RMSE value of 0.296, indicating low prediction errors and high quality of the predictive model. The R^2 value of 0.640 indicates that the model explains about 64% of the variance in the data, which indicates its good performance. Since the data used is purely numerical data, linear regression is considered the most suitable for analyzing this type of data, as it reflects the linear relationship between variables more accurately, compared to other models that

may be less suitable for dealing with numerical data. Despite the good performance of the model, there is room for improving the predictions by introducing additional features or exploring other models.
This holistic analysis not only enhanced our understanding of the UWHVF data but also underscored the importance of employing a diverse set of models in data analysis tasks.

6. Conclusion and Future Work

In conclusion, the integration of Artificial Intelligent techniques in visual field assessment using the HFA represents a significant shift with the potential to greatly enhance ocular health outcomes. By addressing technical, clinical, and ethical challenges, the ophthalmic community can utilize AI to provide more accurate, efficient, and patient-centered care. As AI continues to advance, its role in visual field assessment is likely to expand, offering new opportunities for early diagnosis, personalized treatment, and improved management of ocular diseases.
Therefore, future systems should integrate data about visual field from HFA and incorporate diagnostic modalities such as optical coherence tomography, fundus photography, and genetic data for comprehensive management. These possibly enable the AI-driven diagnosis and treatment recommendation with greater resolution and replicability. Currently, most AI models cannot be adapted to individuals; personalized models may be generated from patient history, demographical data, and patterns in the onset and development of the diseases. Future improvements could come in the form of making the system analyze in real-time during HFA testing. In that case, clinicians will easily give immediate feedback and change the test protocol dynamically to focus on concerns. For clinical acceptance, it is very important to make models more interpretable. More work needs to be performed to develop explainable AI frameworks that can give very transparent insights into the decision-making process involved. Advanced data augmentation, synthetic data generation, and domain adaptation methods are required to make the models robust and generalizable across populations, as visual field data is usually small in size.
The AI systems could be tuned toward predictive modeling to establish the patients who are likely to develop visual field defects even before clinical symptoms become manifest. These are the sorts of pro-active approaches necessary for the revolutionizing of prevention in ophthalmology. Lightweight deep models of AI should be developed that are deployable on low-resources devices to ensure accessibility to such advanced diagnostic tools in remote and underserved regions.

References

1. T. Shyamalee, D. Meedeniya, G. Lim, and M. Karunarathne, “Automated Tool Support for Glaucoma Identification With Explainability Using Fundus Images” IEEE Access, vol. 12, no. January, pp. 17290–17307, 2024, doi: 10.1109/ACCESS.2024.3359698.
2. John Kruper, AdamRichie-Halford, Noah C. Benson, Sendy Caffarra, Julia Owen, Yue Wu, Catherine Egan, Aaron Y. Lee, Cecilia S. Lee, Jason D. Yeatman, Ariel Rokem, & UK Biobank Eye and Vision Consortium, “Convolutional neural network-based classification of glaucoma using optic radiation tissue properties” Commun. Med., vol. 4, no. 1, 2024, doi: 10.1038/s43856-024-00496-w.
3. L. B. Merabet, A. Pascual-Leone, “Neural reorganization following sensory loss: The opportunity of change” Nat. Rev. Neurosci., vol. 11, no. 1, pp. 44–52, 2010, doi: 10.1038/nrn2758.
4. D. Bavelier, H. J. Neville, “Cross-modal plasticity: Where and how?” Nat. Rev. Neurosci., vol. 3, no. 6, pp. 443–452, 2002, doi: 10.1038/nrn848.
5. J. Caprioli, “Glaucoma: A disease of early cellular senescence” Investig. Ophthalmol. Vis. Sci., vol. 54, no. 14, 2013, doi: 10.1167/iovs.13-12716.

6. G. A. Lee, G. Y. X. Kong, and C. H. Liu, "Visual fields in glaucoma: Where are we now?" Clin. Exp. Ophthalmol., vol. 51, no. 2, pp. 162–169, 2023, doi: 10.1111/ceo.14210.

7. Prum, Bruce E, Rosenberg, Lisa F, Gedde, Steven J, Mansberger, Steven L, Stein, Joshua D, Moroi, Sayoko E, Herndon, Leon W, Lim, Michele C, Williams, Ruth D,"Primary Open-Angle Glaucoma" Ophthalmology, vol. 123, no. 1, pp. P41–P111, 2016, doi: 10.1016/j.ophtha.2015.10.053.

8. J. Phu, A. Agar, H. Wang, K. Masselos, and M. Kalloniatis, "Management of open-angle glaucoma by primary eye-care practitioners: toward a personalised medicine approach" Clin. Exp. Optom., vol. 104, no. 3, pp. 367–384, 2021, doi: 10.1111/cxo.13114.

9. R. S. Bodil Gesslein, Magdalena Naumovska, Olof Neumann, Dimitrios Bizios, Boel Bengtsson, Peter Siesjö, Erik Uvelius, Björn Hammar, "Acta Ophthalmologica - 2023 - Gesslein - Comparison of perimetric 24-2 and 30-2 test patterns in detecting visual field.pdf." Acta Ophthalmologica, p. 8, 2022. [Online]. Available: https://pubmed.ncbi.nlm.nih.gov/37452447/

10. Henry D. Jampel,Kuldev Singh, Shan C. Lin, Teresa C. Chen, Brian A. Francis, Elizabeth Hodapp, John R. Samples, Scott D. Smith, "Assessment of visual function in glaucoma: A report by the American academy of ophthalmology" Ophthalmology, vol. 118, no. 5, pp. 986–1002, 2011, doi: 10.1016/j.ophtha.2011.03.019.

11. J. Phu, S. K. Khuu, M. Yapp, N. Assaad, M. P. Hennessy, and M. Kalloniatis, "The value of visual field testing in the era of advanced imaging: clinical and psychophysical perspectives" Clin. Exp. Optom., vol. 100, no. 4, pp. 313–332, 2017, doi: 10.1111/cxo.12551.

12. Schiefer U, Papageorgiou E, Sample Pamela A, Pascual John P, Selig Bettina, Krapp E, and Paetzold J, "Spatial pattern of glaucomatous visual field loss obtained with regionally condensed stimulus arrangements" Investig. Ophthalmol. Vis. Sci., vol. 51, no. 11, pp. 5685–5689, 2010, doi: 10.1167/iovs.09-5067.

13. J. M. Khoury, S. P. Donahue, P. J. Lavin, and J. C. Tsai, "Comparison of 24-2 and 30-2 perimetry in glaucomatous and nonglaucomatous optic neuropathies" J. neuro-ophthalmology Off. J. North Am. Neuro-Ophthalmology Soc., vol. 19, no. 2, pp. 100–108, Jun. 1999.

14. A.Heijl ,V. M. Patella, X. L. Chong, A. Iwase, K.L. Christopher. A. Tuulonen, C. L. Gary, T. Callan, B. Bengtsson, "A New SITA Perimetric Threshold Testing Algorithm: Construction and a Multicenter Clinical Study" Am. J. Ophthalmol., vol. 198, pp. 154–165, 2019, doi: 10.1016/j.ajo.2018.10.010.

15. J. Phu, S. K. Khuu, A. Agar, and M. Kalloniatis, "Clinical Evaluation of Swedish Interactive Thresholding Algorithm–Faster Compared With Swedish Interactive Thresholding Algorithm–Standard in Normal Subjects, Glaucoma Suspects, and Patients With Glaucoma" Am. J. Ophthalmol., vol. 208, pp. 251–264, 2019, doi: 10.1016/j.ajo.2019.08.013.

16. Yi Sun, Clarissa Lin, Michael Waisbourd, Feyzahan Ekici, Elif Erdem, Sheryl S. Wizov, Lisa A. Hark, George L. Spaeth, "The Impact of Visual Field Clusters on Performance-based Measures and Vision-Related Quality of Life in Patients with Glaucoma" Am. J. Ophthalmol., vol. 163, pp. 45–52, 2016, doi: 10.1016/j.ajo.2015.12.006.

17. D. M. Blumberg, C.G. De Moraes, A.J Prager, Yu Qi, L. Al-Aswad, A.G. Cioffi, J.M Liebmann, D.C. Hood, "Association between undetected 10-2 visual field damage and vision-related quality of life in patients with glaucoma" JAMA Ophthalmol., vol. 135, no. 7, pp. 742–747, 2017, doi: 10.1001/jamaophthalmol.2017.1396.

18. Y. Yamazaki, K. Sugisaki, M. Araie, H. Murata, A. Kanamori, T. Inoue, S. Ishikawa, K. Yoshikawa, H. Maeda, Y. Yamada, A. Negi, M. Inatani, H. Tanihara, S. Okinami, K. Mizuki, K. Mishima, K. Uchida, S. Matsumoto, "Relationship between Vision-Related Quality of Life and Central 10° of the Binocular Integrated Visual Field in Advanced Glaucoma" Sci. Rep., vol. 9, no. 1, pp. 1–9, 2019, doi: 10.1038/s41598-019-50677-0.

19. A. White and I. Goldberg, “Guidelines for the collaborative care of glaucoma patients and suspects by ophthalmologists and optometrists in Australia” Clin. Exp. Ophthalmol., vol. 42, no. 2, pp. 107–117, 2014, doi: 10.1111/ceo.12270.
20. D. C. H. Ilana Traynis, Carlos G. De Moraes, Ali S. Raza, Jeffrey M. Liebmann, Robert Ritch, “The Prevalence and Nature of Early Glaucomatous Defects in the Central 10° of the Visual Field” JAMA Ophthalmol, vol. 23, no. 1, pp. 1–7, 2008, doi: 10.1001/jamaophthalmol.2013.7656.
21. J. M. L. C. Gustavo De Moraes, Donald C. Hood, Abinaya Thenappan, Christopher A. Girkin, Felipe A. Medeiros, Robert N. Weinreb, Linda M. Zangwill, “24-2 Visual Fields Miss Central Defects Shown on 10-2 Tests in Glaucoma Suspects, Ocular Hypertensives, and Early Glaucoma” Ophthalmology., vol. 176, no. 1, pp. 139–148, 2016, doi: 10.1016/j.ophtha.2017.04.021.24-2.
22. J. Phu and M. Kalloniatis, “Ability of 24-2C and 24-2 Grids to Identify Central Visual Field Defects and Structure-Function Concordance in Glaucoma and Suspects” Am. J. Ophthalmol., vol. 219, pp. 317–331, 2020, doi: 10.1016/j.ajo.2020.06.024.
23. M. Sullivan-Mee, M. T. Karin Tran, D. Pensyl, G. Tsan, and S. Katiyar, “Prevalence, Features, and Severity of Glaucomatous Visual Field Loss Measured with the 10-2 Achromatic Threshold Visual Field Test” Am. J. Ophthalmol., vol. 168, pp. 40–51, 2016, doi: 10.1016/j.ajo.2016.05.003.
24. M. E. West, G. P. Sharpe, Donna M. Hutchison, Paul E. Rafuse, Lesya M. Shuba, Marcelo T. Nicolela, Jayme R. Vianna, Balwantray C. Chauhan, “Value of 10-2 Visual Field Testing in Glaucoma Patients with Early 24-2 Visual Field Loss” Ophthalmology, vol. 128, no. 4, pp. 545–553, 2021, doi: 10.1016/j.ophtha.2020.08.033.
25. Z. Wu, F. A. Medeiros, R. N. Weinreb, L.M. Zangwill, S. Diego, L. Jolla, Royal Victorian Eye, Ear Hospital, East Melbourne, North Carolina, “HHS Public Access” pp. 10–17, 2019, doi: 10.1016/j.ajo.2018.08.010.Performance.
26. A. Orbach, G.S. Ang, A.S. Camp, D.S. Welsbie, F.A.Medeiros, C.A. Girkin, M.A. Fazio, W.H. Oh, R.N. Weinreb, L.M. Zangwill, Z. Wu, “Qualitative Evaluation of the 10-2 and 24-2 Visual Field Tests for Detecting Central Visual Field Abnormalities in Glaucoma” Am. J. Ophthalmol., vol. 229, pp. 26–33, 2021, doi: 10.1016/j.ajo.2021.02.015.
27. J. Phu and M. Kalloniatis, “Comparison of 10-2 and 24-2C Test Grids for Identifying Central Visual Field Defects in Glaucoma and Suspect Patients,” Ophthalmology, vol. 128, no. 10, pp. 1405–1416, 2021, doi: 10.1016/j.ophtha.2021.03.014.
28. J. Phu and M. Kalloniatis, “A Strategy for Seeding Point Error Assessment for Retesting (SPEAR) in Perimetry Applied to Normal Subjects, Glaucoma Suspects, and Patients With Glaucoma” Am. J. Ophthalmol., vol. 221, pp. 115–130, 2021, doi: 10.1016/j.ajo.2020.07.047.
29. J. Phu and M. Kalloniatis, “Viability of Performing Multiple 24-2 Visual Field Examinations at the Same Clinical Visit: The Frontloading Fields Study (FFS)” Am. J. Ophthalmol., vol. 230, pp. 48–59, 2021, doi: 10.1016/j.ajo.2021.04.019.
30. D. T. Hogarty, D. A. Mackey, and A. W. Hewitt, “Current state and future prospects of artificial intelligence in ophthalmology: a review” Clin. Exp. Ophthalmol., vol. 47, no. 1, pp. 128–139, 2019, doi: 10.1111/ceo.13381.
31. M. M. Hasan, J. Phu, A. Sowmya, E. Meijering, and M. Kalloniatis, “Artificial intelligence in the diagnosis of glaucoma and neurodegenerative diseases” Clin. Exp. Optom., vol. 107, no. 2, pp. 130–146, 2024, doi: 10.1080/08164622.2023.2235346.
32. M. Gazanchian and N. M. Jansonius, “Effect of Nonoverlapping Visual Field Defects on Vision-related Quality of Life in Glaucoma” Ophthalmol. Glaucoma, pp. 1–9, 2024, doi: 10.1016/j.ogla.2024.01.007.
33. Elliot B. Werner, “Manual of Visual Fields, Illustrate”. Churchill Livingstone, 1991, 1991.

34. P. H. Artes, M. T. Nicolela, R. P. LeBlanc, and B. C. Chauhan, "Visual field progression in glaucoma: Total versus pattern deviation analyses" Investig. Ophthalmol. Vis. Sci., vol. 46, no. 12, pp. 4600–4606, 2005, doi: 10.1167/iovs.05-0827.

35. S. R. K. Tripathy., "Humphrey Visual Field" August 25, 2023. [Online]. Available: https://www.ncbi.nlm.nih.gov/books/NBK585112/

36. B. Y. M. Y. Kahook and R. J. Noecker, "How do you interpret a 24-2 humphrey visual field printout?" Glaucoma Today, no. December, pp. 57–59, 2007.

37. Z. Zhou, B. Li, Jinyu Su, X. Fan, L. Chen, S. Tang, J. Zheng, T. Zhang, Z. Meng, Z. Chen, H. Deng, Jianmin Hu, J. Zhao, "An artificial intelligence model for the simulation of visual effects in patients with visual field defects" Ann. Transl. Med., vol. 8, no. 11, pp. 703–703, Jun. 2020, doi: 10.21037/atm.2020.02.162.

38. K. Gupta, A. Thakur, M. Goldbaum, and S. Yousefi, "Glaucoma Precognition: Recognizing Preclinical Visual Functional Signs of Glaucoma."

39. Z. Guo, Y.H. Kwon, K. Lee, K. Wang, A. Wahle, W. L.M. Alward, J.H. Fingert, D.I. Bettis, C.A. Johnson, M.K. Garvin, M. Sonka, M.D. Abràmoff, "Optical coherence tomography analysis-based prediction of Humphrey 24-2 visual field thresholds in patients with glaucoma" Investig. Ophthalmol. Vis. Sci., vol. 58, no. 10, pp. 3975–3985, Aug. 2017, doi: 10.1167/iovs.17-21832.

40. J.C. Wen, C.S. Lee, P.A. Keane, S. Xiao, A.S. Rokem, P. P. Chen, Yue Wu, A. Y. Lee, "Forecasting future humphrey visual fields using deep learning" PLoS One, vol. 14, no. 4, Apr. 2019, doi: 10.1371/journal.pone.0214875.

41. M. Saifee, J. Wu, Y. Liu, P. Ma, J. Patlidanon, Y. Yu, G.S. Ying, Y. Han, "Development and Validation of Automated Visual Field Report Extraction Platform Using Computer Vision Tools" Front. Med., vol. 8, no. April, pp. 1–13, 2021, doi: 10.3389/fmed.2021.625487.

42. M. Eslami, S. Kazeminasab, V. Sharma, Y. Li, M. Fazli, M. Wang, N. Zebardast, T. Elze, "PyVisualFields: A Python Package for Visual Field Analysis" Transl. Vis. Sci. Technol., vol. 12, no. 2, pp. 1–9, 2023, doi: 10.1167/tvst.12.2.6.

43. G. Montesano, A. Chen, R. Lu, C. S. Lee, and A. Y. Lee, "UWHVF: A Real-World, Open-Source Dataset of Perimetry Tests from the Humphrey Field Analyzer at the University of Washington," Transl. Vis. Sci. Technol., vol. 11, no. 1, pp. 1–8, 2022, doi: 10.1167/TVST.11.1.1.

44. "Harvard Ophthalmology AI Lab Dataset." Accessed: Jun. 17, 2024. [Online]. Available: ("https://ophai.hms.harvard.edu/datasets/")

45. C. Nakayama, L. F., Goncalves, M., Zago Ribeiro, L., Santos, H., Ferraz, D., Malerbi, F., Celi, L. A., & Regatieri, "A Brazilian Multilabel Ophthalmological Dataset (BRSET)," PhysioNet, 2023, doi: https://doi.org/10.13026/xcxw-8198.